



Method for real-time self-calibrating GLONASS code inter-frequency bias and improvements on single point positioning

Liang Chen^{1,2} · Min Li^{1,3} · Zhigang Hu^{1,3} · Chenghe Fang² · Changjiang Geng² · Qile Zhao^{1,3} · Chuang Shi^{4,5}

Received: 23 February 2018 / Accepted: 11 August 2018 / Published online: 17 August 2018
© Springer-Verlag GmbH Germany, part of Springer Nature 2018

Abstract

Utilization of frequency-division multiple access (FDMA) leads to GLONASS pseudorange and carrier phase observations suffering from variable levels inter-frequency bias (IFB). The bias related with carrier phase can be absorbed by ambiguities. However, the unequal code inter-frequency bias (cIFB) will degrade the accuracy of pseudorange observations, which will affect positioning accuracy and convergence of precise point positioning (PPP) when including GLONASS satellites. Based on observations made on un-differenced (UD) ionospheric-free combinations, GLONASS cIFB parameters are estimated as a constant to achieve GLONASS cIFB real-time self-calibration on a single station. A total of 23 stations, with different manufacturing backgrounds, are used to analyze the characteristics of GLONASS cIFB and its relationship with variable receiver hardware. The results show that there is an obvious common trend in cIFBs estimated using broadcast ephemeris for all of the different manufacturers, and there are unequal GLONASS inter-satellite cIFB that match brand manufacture. In addition, a particularly good consistency is found between self-calibrated receiver-dependent GLONASS cIFB and the IFB products of the German Research Centre for Geosciences (GFZ). Via a comparative experiment, it is also found that the algorithm of cIFB real-time self-calibration not only corrects receiver-dependent cIFB, but can moreover eliminate satellite-dependent cIFB, providing more stable results and further improving global navigation satellite system (GNSS) point positioning accuracy. The root mean square (RMS) improvements of single GLONASS standard point positioning (SPP) reach up to 54.18 and 53.80% in horizontal and vertical direction, respectively. The study's GLONASS cIFB self-estimation can realize good self-consistency between cIFB and stations, working to further promote convergence efficiency relative to GPS + GLONASS PPP. An average improvement percentage of 19.03% is observed, realizing a near-consistent accuracy with GPS + GLONASS fusion PPP.

Keywords GLONASS · GPS · Code inter-frequency bias · Code self-calibration · SPP and PPP · Performance improvement

Introduction

The American Global Positioning System (GPS) has been operating for more than 20 years. Russia has also put up a full constellation of 24 of GLONASS satellites that began operation on December 8, 2011. China's BeiDou-2 satellite system has likewise provided service for the Asia-Pacific area for about 5 years until now. The European Galileo also declared initial service on December 2016. With more satellites joining the family of global navigation satellite systems (GNSSs), multi-GNSS fusion positioning research and application are becoming increasingly popular. In this vein, as a result of frequency-division multiple access (FDMA) utilization, GLONASS pseudorange and carrier phase observations suffer from inter-frequency bias (IFB) (Wanninger and Wallstab-Freitag 2007). Specifically, the bias related to

✉ Min Li
limin@whu.edu.cn

¹ GNSS Research Center, Wuhan University, 129 Luoyu Road, Wuhan 430079, China

² GNSS Engineering Center, China Academy of Aerospace Electronics Technology, 1 Fengying East Road, Beijing 100094, China

³ National Engineering Center for Satellite Positioning System, 129 Luoyu Road, Wuhan 430079, China

⁴ School of Electronic and Information Engineering, Beihang University, 37 Xueyuan Road, Beijing 100191, China

⁵ Collaborative Innovation Center of Geospatial Technology, 37 Xueyuan Road, Beijing 100191, China

pseudorange is referred to as code IFB (cIFB), and another related bias in carrier phase is referred to as uncalibrated phase delay (UPD) (Ge et al. 2008; Li et al. 2013).

In the standard point positioning (SPP) that is based on pseudorange, satellite-dependent cIFB, commonly called time group delay (TGD), is initially provided by the control segments of GNSS (IS-GPS-200G 2013; BeiDou SIS ICD 2017; Galileo OS SIS ICD 2016). In the GLONASS interface control document (ICD), some description is provided regarding equipment group delay (EGD), which is defined as a delay between the transmitted radio frequency signal at phase center of the transmitting antenna and a signal at the output of the onboard time/frequency standard and does not exceed 8 ns for GLONASS satellite and 2 ns for GLONASS-M satellite (GLONASS ICD 2008).

However, the corrected parameters of such EGD are not provided in the GLONASS broadcast ephemeris data, which works to affect GLONASS SPP performance significantly. Even though multi-GNSS satellite-dependent differential code bias (DCB) has been provided by Multi-GNSS Experiment (M-GEX) (Montenbruck et al. 2017), it only includes the code inter-frequency channel bias for GLONASS ionospheric-free observations, which can only be used with precise orbit and clock products at the same time. It is difficult for real-time users to obtain such products. In Ge et al. (2017), the transformational relationship between TGD and DCB for multi-GNSS were derived, and the impact on multi-GNSS fusion positioning of TGD, as provided by broadcast ephemeris data, and DCB, as provided by the M-GEX, were compared and analyzed comprehensively.

In precise point positioning (PPP) (Zumberge et al. 1997) that is based on precise orbit and clock products, and as provided by the International GNSS Service (IGS) (<http://www.igs.org/products>), the satellite-dependent cIFB are included in precise satellite clock products generated by ionospheric-free observations (Montenbruck et al. 2017). However, in PPP ambiguity resolution, wide-lane ambiguity is first resolved using pseudorange observations by means of the Hatch-Melbourne-Wübbena combination (Hatch 1982; Ge et al. 2008), and fixing efficiency will depend on the noise of the pseudorange observations (Ge et al. 2008; Geng et al. 2010a). Unequal GLONASS receiver-dependent cIFB cannot be absorbed completely by receiver clocks, and remaining residual bias will degrade pseudorange observations accuracy.

An updated list of a priori corrections for the differential carrier phase inter-frequency bias found in the receivers of different manufacturers has been provided by past research. The results were compiled by analyzing 133 individual GPS/GLONASS receivers, from 19 receiver types, as produced by nine different manufacturers (Wanninger 2012). However, it must be noted that those corrections do not address receiver inter-frequency bias in GLONASS code observations. In Shi

et al. (2013), undifferenced (UD) receiver-dependent cIFB of GLONASS were estimated using 133 receivers from five manufacturers, based on precision products that were provided by the European Space Agency. After calibrating the cIFB accordingly, the positioning accuracy of SPP as well as the convergence performance of PPP was improved significantly. The receiver-dependent GLONASS IFB, as based on the ionospheric-free observations of the M-GEX stations, are available as products in a preliminary version of the Bias-SINEX format by the German Research Centre for Geosciences (GFZ) (<ftp://ftp.gfz-potsdam.de/pub/GNSS/products/mgex/www>) (Montenbruck et al. 2017).

For this study, the GLONASS cIFB real-time estimation and self-calibration model are presented below. Thereafter, data processing strategies are introduced. Details on the characteristics of the cIFB estimated by broadcast ephemeris data as well as for precision products are described afterward. Then, the GLONASS cIFB self-calibration and its effects on positioning are analyzed. Lastly, a summary of the results and corresponding conclusions are presented.

A cIFB real-time estimation and self-calibration model

Ionospheric-free combination observations are used commonly in dual-frequency data processing to eliminate the ionospheric delay. If a unified time reference is chosen, the UD observation equation for ionospheric-free combination in multi-GNSS fusion positioning for GPS, GLONASS, BeiDou, or Galileo is as follows (Li et al. 2015):

$$\begin{cases} PC_i^G = \rho_i^G + dt + b_{PC}^G - dT_i^G - B_{i,PC}^G + d_{i,trop}^G + \epsilon_{i,PC}^G \\ LC_i^G = \rho_i^G + dt + b_{LC}^G - dT_i^G - B_{i,LC}^G + N_i^G + d_{i,trop}^G + \epsilon_{i,LC}^G \\ PC_{j,PC}^R = \rho_j^R + dt + b_{j,PC}^R - dT_j^R - B_{j,PC}^R + d_{j,trop}^R + \epsilon_{j,PC}^R \\ LC_{j,LC}^R = \rho_j^R + dt + b_{j,LC}^R - dT_j^R - B_{j,LC}^R + N_j^R + d_{j,trop}^R + \epsilon_{j,LC}^R \\ PC_{k,PC}^C = \rho_k^C + dt + b_{PC}^C - dT_k^C - B_{k,PC}^C + d_{k,trop}^C + \epsilon_{k,PC}^C \\ LC_{k,LC}^C = \rho_k^C + dt + b_{LC}^C - dT_k^C - B_{k,LC}^C + N_k^C + d_{k,trop}^C + \epsilon_{k,LC}^C \\ PC_{m,PC}^E = \rho_m^E + dt + b_{PC}^E - dT_m^E - B_{m,PC}^E + d_{m,trop}^E + \epsilon_{m,PC}^E \\ LC_{m,LC}^E = \rho_m^E + dt + b_{LC}^E - dT_m^E - B_{m,LC}^E + N_m^E + d_{m,trop}^E + \epsilon_{m,LC}^E \end{cases} \quad (1)$$

where G , R , C , and E represent one GPS, GLONASS, BeiDou, or Galileo satellite, respectively; i , j , k , and m denote the i th GPS, the j th GLONASS, the k th BeiDou, and the m th Galileo satellite at the same epoch, respectively; PC , LC , and N represent pseudorange, carrier phase, and ambiguity of ionospheric-free measurements, respectively; ρ is the geometric distance from a given satellite to the receiver; dt and dT represent receiver and satellite clock offset, respectively;

d_{trop} denotes tropospheric delay; ϵ denotes the observation noise; b and B represent the receiver-dependent and satellite-dependent signal delay bias, respectively. The bias related to the pseudorange is noted as cIFB. The bias related to the carrier phase is noted as UPD. Because of the differences in frequency, GLONASS pseudorange and carrier phase observations suffer from cIFB. As such, the subscript j is added to the receiver-dependent and satellite-dependent cIFB to distinguish the GLONASS inter-satellite cIFB.

In the procedure of positioning, the satellite orbit and clock offset is obtained from broadcast ephemeris data or precise orbit and clock products provided by IGS. B_{PC} , the satellite-dependent cIFB in ionospheric-free observations, can also be calculated using the broadcast TGD parameters taken from the broadcast ephemeris data (Ge et al. 2017) or simply ignored if one is using the precise orbit and clock products provided IGS. This is so because such bias is included in the precise satellite clock calculations generated by ionospheric-free observations (Schaer et al. 1998).

For this study, GPS time is chosen as the time reference. The system time offset to GPS time, dt_{sys} , should be introduced when using clock products with a variable time reference. Considering the initial information for normal equation will be provided primarily by pseudorange observations, the GPS receiver-dependent cIFB (b_{PC}^G) and the receiver clock offset (dt) are merged as $d\tilde{t} = dt + b_{PC}^G$. Thus, the linearized equation can be simplified as follows:

$$\begin{cases} v_{i,PC}^G = \mathbf{u}_i^G \cdot \mathbf{dx} + d\tilde{t} + d_{i,trop}^G - l_{i,PC}^G \\ v_{i,LC}^G = \mathbf{u}_i^G \cdot \mathbf{dx} + d\tilde{t} + (b_{LC}^G - b_{PC}^G) - B_{i,LC}^G + N_i^G + d_{i,trop}^G - l_{i,LC}^G \\ v_{j,PC}^R = \mathbf{u}_j^R \cdot \mathbf{dx} + d\tilde{t} + dt_{sys}^{R-G} + (b_{j,PC}^R - b_{PC}^G) + d_{j,trop}^R - l_{j,PC}^R \\ v_{j,LC}^R = \mathbf{u}_j^R \cdot \mathbf{dx} + d\tilde{t} + dt_{sys}^{R-G} + (b_{j,LC}^R - b_{PC}^G) - B_{j,LC}^R + N_j^R + d_{j,trop}^R - l_{j,LC}^R \\ v_{k,PC}^C = \mathbf{u}_k^C \cdot \mathbf{dx} + d\tilde{t} + dt_{sys}^{C-G} + (b_{PC}^C - b_{PC}^G) + d_{k,trop}^C - l_{k,PC}^C \\ v_{k,LC}^C = \mathbf{u}_k^C \cdot \mathbf{dx} + d\tilde{t} + dt_{sys}^{C-G} + (b_{LC}^C - b_{PC}^G) - B_{k,LC}^C + N_k^C + d_{k,trop}^C - l_{k,LC}^C \\ v_{m,PC}^E = \mathbf{u}_m^E \cdot \mathbf{dx} + d\tilde{t} + dt_{sys}^{E-G} + (b_{PC}^E - b_{PC}^G) + d_{m,trop}^E - l_{m,PC}^E \\ v_{m,LC}^E = \mathbf{u}_m^E \cdot \mathbf{dx} + d\tilde{t} + dt_{sys}^{E-G} + (b_{LC}^E - b_{PC}^G) - B_{m,LC}^E + N_m^E + d_{m,trop}^E - l_{m,LC}^E \end{cases} \quad (2)$$

The symbol v denotes the residuals; \mathbf{u} is the unit vector of the direction from receiver to satellite; \mathbf{dx} denotes the vector of receiver position increments, relative to a priori position which is used for linearization; l is the difference between PC, LC, and geometric distance from the satellite to the receiver.

Note the combinations

$$IFB_j^{R-G} = dt_{sys}^{R-G} + b_{j,PC}^R - b_{PC}^G \quad (3)$$

$$ISB^{B-G} = dt_{sys}^{C-G} + b_{PC}^C - b_{PC}^G \quad (4)$$

$$ISB^{E-G} = dt_{sys}^{E-G} + b_{PC}^E - b_{PC}^G \quad (5)$$

The IFB and ISB in (3)–(5) are common parameters for pseudorange and carrier phase observations. Some signal delay bias combinations in pseudorange and carrier phase in the receiver and satellite can be absorbed by ambiguities if the ambiguities are not fixed. As such, the linearization of (2) can be expressed as follows:

$$\begin{cases} v_{i,PC}^G = \mathbf{u}_i^G \cdot \mathbf{dx} + d\tilde{t} + d_{i,trop}^G - l_{i,PC}^G \\ v_{i,LC}^G = \mathbf{u}_i^G \cdot \mathbf{dx} + d\tilde{t} + \tilde{N}_i^G + d_{i,trop}^G - l_{i,LC}^G \\ v_{j,PC}^R = \mathbf{u}_j^R \cdot \mathbf{dx} + d\tilde{t} + IFB_j^{R-G} + d_{j,trop}^R - l_{j,PC}^R \\ v_{j,LC}^R = \mathbf{u}_j^R \cdot \mathbf{dx} + d\tilde{t} + IFB_j^{R-G} + \tilde{N}_j^R + d_{j,trop}^R - l_{j,LC}^R \\ v_{k,PC}^C = \mathbf{u}_k^C \cdot \mathbf{dx} + d\tilde{t} + ISB^{C-G} + d_{k,trop}^C - l_{k,PC}^C \\ v_{k,LC}^C = \mathbf{u}_k^C \cdot \mathbf{dx} + d\tilde{t} + ISB^{C-G} + \tilde{N}_k^C + d_{k,trop}^C - l_{k,LC}^C \\ v_{m,PC}^E = \mathbf{u}_m^E \cdot \mathbf{dx} + d\tilde{t} + ISB^{E-G} + d_{m,trop}^E - l_{m,PC}^E \\ v_{m,LC}^E = \mathbf{u}_m^E \cdot \mathbf{dx} + d\tilde{t} + ISB^{E-G} + \tilde{N}_m^E + d_{m,trop}^E - l_{m,LC}^E \end{cases} \quad (6)$$

where $\tilde{N} = N - b_{PC} + b_{LC} - B_{LC}$.

The IFB parameters can be estimated as constant parameters in multi-GNSS SPP or PPP by (6). In (3), the IFB

parameters include some public parameters, such as the GLONASS to GPS system time offset (dt_{sys}^{R-G}) and the GPS receiver-dependent cIFB (b_{PC}^G). Equation (3) can be rewritten to include $\bar{b}_{j,PC}^R$, the mean of all GLONASS satellite receiver-dependent cIFB, which are the same for all GLONASS satellites. Assuming the GLONASS to GPS system time offset and GPS receiver-dependent cIFB remain stable over 24 h (Dach et al. 2006), $\hat{b}_{j,PC}^R$, which is the cIFB of GLONASS,

can be separated by subtracting the mean of all IFB_j^{R-G} , namely:

$$\hat{b}_{j,PC}^R = IFB_j^{R-G} - \frac{1}{n} \sum_{j=1}^n IFB_j^{R-G}, \tag{7}$$

where n is the number of GLONASS satellites.

As mentioned above, the corrected parameters of EGD are not provided in GLONASS broadcast ephemeris data. In GLONASS point positioning, the cIFB can also be obtained as follows:

$$\begin{cases} v_{j,PC}^R = \mathbf{u}_j^R \cdot \mathbf{dx} + dt + IFB_j^R + d_{j,trop}^R - I_{j,PC}^R \\ v_{j,LC}^R = \mathbf{u}_j^R \cdot \mathbf{dx} + dt + IFB_j^R + \tilde{N}_j^R + d_{j,trop}^R - I_{j,LC}^R \end{cases}, \tag{8}$$

where $IFB_j^R = b_{j,PC}^R - B_{j,PC}^R$ and $\tilde{N}_j^R = N_j^R - (b_{j,PC}^R - B_{j,PC}^R) + (b_{j,LC}^R - B_{j,LC}^R)$. If one uses only the ionospheric-free pseudorange combination in (8), the IFB parameters can be estimated as constant parameters at each epoch via a filter algorithm for a single station, which brings about GLONASS cIFB self-calibration into the SPP mode. This process is same in the PPP mode with GLONASS satellites when using ionospheric-free combinations of pseudorange and phase observations. As such, the IFB parameter found for GLONASS SPP using broadcast ephemeris data includes not only the receiver-dependent cIFB, but also the satellite-dependent cIFB (also called EGD or TGD). However, receiver-dependent cIFB is only included when using IGS precise orbit and clock products.

On account of relying solely on your own satellite observations and the broadcast ephemeris, rather than the observations from other stations or the products from other organizations, the algorithm above can realize self-calibration in GLONASS cIFB at a single station independently. Moreover, because the GLONASS cIFB parameters are estimated as a constant, there may be an obvious convergence with the accumulation of observations.

Real-time cIFB estimation

Based on UD ionospheric-free observations, the real-time GLONASS cIFB at each epoch can be estimated. For this, the elevation mask of satellites is set as seven degrees while the sampling rate is set at 30 s. The phase center offset and phase center variation for satellites and stations are corrected by values listed in IGS14.atx. The initial value for the tropospheric delay is provided by the Saastamoinen model, while the residual terms are estimated as a random walk for each epoch. The ambiguities are estimated as float, and the ISB

and cIFB parameters are estimated as constant parameters (Li et al. 2015). Square-root information filtering is used for adjustment (Bierman 1977).

Data preparation

To analyze the characteristics of GLONASS cIFB from various manufactures and hardware, 23 stations equipped with eight receiver types and 12 firmware produced by six different manufacturers are used to estimate GLONASS cIFB via the pseudorange observations as presented in (8). The receiver, firmware, and antenna types are presented in detail in Table 1 and the corresponding distribution is presented in Fig. 1. The test data are selected from Day of Year (DOY) 200–300, 2017.

Characteristics of GLONASS cIFB from Broadcast Ephemeris Data

Figure 2 shows the 24 h time series comparison for the GLONASS cIFB, as estimated by broadcast ephemeris data and GFZ multi-GNSS precision products, for station METG in SPP. As with the ambiguities for phase observations, there is first a significant convergence period, but thereafter all GLONASS cIFB stabilize.

As analyzed earlier, the IFB parameter is estimated by broadcast ephemeris data that includes receiver-dependent and satellite-dependent cIFB, so that the variation amplitude found in Fig. 2 will be larger than as in the case estimated by GFZ products.

Figure 3 shows the variation in cIFB, as estimated by the broadcast ephemeris data taken from DOY 200 to 300 in 2017, for the 23 stations mentioned in Table 1. From the sub-figures, it can be seen that there is an obvious common trend for all manufacturers. This may be caused by satellite-dependent cIFB, which is a commonality in IFB parameters. The specific characteristics of GLONASS cIFB noted above can also be obtained using the methodology noted in Shi et al. (2013). In addition, it must be noted that the inter-satellites cIFB for some manufacturers changes significantly, as is the case with Leica and TPS. These differences can reach magnitudes of up to about 10 m (Fig. 3-Leica, TPS). However, all of the GLONASS cIFB for Trimble are found to stabilize from -4.0 to 4.0 m, which is conducive to performance improvement in GLONASS positioning, since the mean of all GLONASS cIFB can be absorbed by the receiver clock parameters.

Figure 3 shows that most standard deviations (STDs) of GLONASS cIFB are less than 1.30 m, except for the stations equipped with Javad. According to the statistics, the average STD of all 23 stations is 1.32 m, which is limited by the broadcast ephemeris accuracy for GLONASS.

Table 1 Information on GNSS receiver type, firmware, and antenna type at the test stations

Manufacturer	Receiver type	Firmware	Antenna Type	Station
Leica	GRX1200+ GNSS	9.20	LEIAR25.R4	BZRG
	GR25	4.02/4.11	TRM57971.00	GRAC
	GR25	4.02/4.11	LEIAR25.R4	HKSL
	GR25	3.11	LEIAR25.R4	HOFN
SEPT	POLARX4	2.9.5	SEPCHOKE_MC	CEBR
	POLARX4	2.9.5	SEPCHOKE_MC	KOUR
	POLARX4	2.9.5	LEIAR25.R4	MAL2
TPS	NET-G3A	3.6	TRM59800.00	ALBH
	NET-G3A	3.6	TPSCR.G3	FRDN
	NET-G3A	3.6	TPSCR.G3	HLFX
	NET-G3A	3.5	TPSCR.G3	IQAL
Trimble	NETR5	4.85	TRM55971.00	ASPA
	NETR9	4.85	ASH700936D_M	ANTC
	NETR9	4.85	TRM57971.00	BRST
	NETR9	4.85	TRM57971.00	LMMF
JAVAD	TRE_G3TH DELTA	3.6.3	AOAD/M_T	ALGO
	TRE_G3TH DELTA	3.6.4	ASH701945G_M	KOKV
	TRE_G3TH DELTA	3.6.4	JAVRINGANT_DM	MKEA
	TRE_G3TH DELTA	3.6.3	AOAD/M_T	NRC1
JPS	EGGDT	2.7.0	AOAD/M_T	GODZ
	EGGDT	2.7.0	AOAD/M_T	GOLD
	EGGDT	2.7.0	TPSCR3_GGD	TIXI

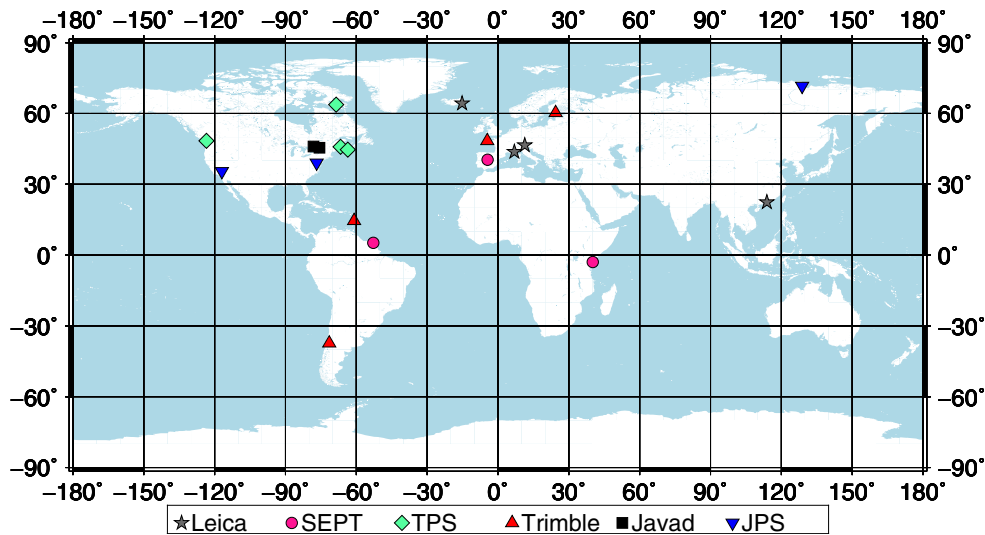


Fig. 1 Distribution of GNSS stations. Symbols: grey star (Leica), pink circle (SEPT), green rhombus (TPS), red triangle (Trimble), black square (Javad), blue inverted triangle (JPS)

For comparison, it should note that the STD for receiver-dependent cIFB in the daily products provided by GFZ is about 2 m.

Accuracy of cIFB from Precision Products Compared to GFZ Products

Using precise orbit and clock products, receiver-dependent cIFB can be obtained in GLONASS single positioning. To

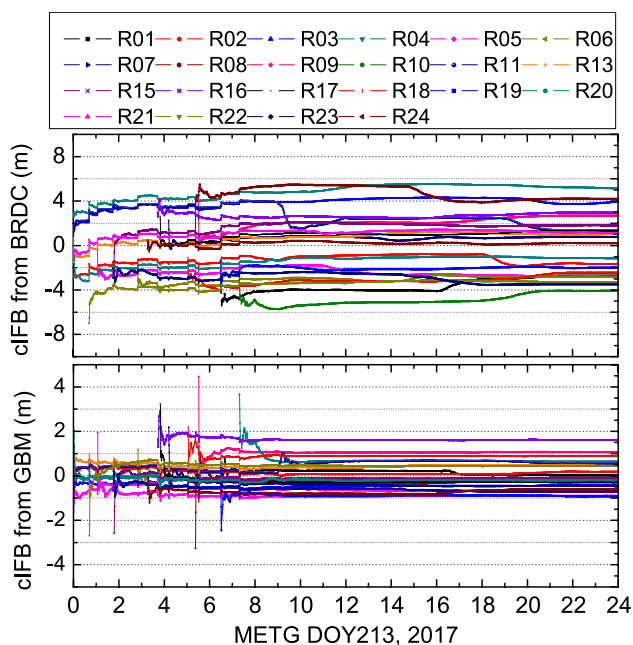


Fig. 2 Time Series for the GLONASS cIFB estimates for station METG over 24 h. Top: GLONASS cIFB estimated as broadcast ephemeris. Bottom: GLONASS cIFB estimated using GFZ precision products. The cIFB estimates using broadcast ephemeris are larger than those estimated by GFZ products

analyze the characteristics of receiver-dependent GLONASS cIFB, precise multi-GNSS orbit and clock products provided by GFZ were chosen (Deng et al. 2017) in GLONASS SPP.

The receiver-dependent GLONASS cIFB have been provided by GFZ which can be used to verify the accuracy of receiver-dependent cIFB as estimated in this section. It must be noted that the cIFB products from GFZ are derived by fixing the IFB of one station instead of adding the zero-mean conditions for all the IFBs to separate the cIFB from GLONASS receiver clock offset (Deng et al. 2017). Thus, the mean of all GLONASS cIFB for one station should be deducted.

A total of 13 common stations from Table 1 and GFZ products are selected to verify the accuracy of the receiver-dependent GLONASS cIFB, as well as the RMS of GLONASS cIFB, relative to the GFZ products from DOY 200 to 206 in 2017. The results are presented in Fig. 4. Here it is found that most measures for RMS are less than 0.6 m and that the mean of the RMS for all stations and GLONASS satellites is 0.26 m. A good consistency is observed between receiver-dependent self-calibrated GLONASS cIFB and GFZ products.

Effect of GLONASS cIFB Self-calibration on Positioning

As noted above, the differences in receiver-dependent and satellite-dependent GLONASS cIFB can reach up to several meters, which should be considered in GNSS positioning, especially for GLONASS satellites. The single positioning accuracy and performance, both before and after self-calibrating for GLONASS cIFB, are analyzed below.

cIFB Self-calibration on SPP

Figures 5 and 6 show the GLONASS ionospheric-free combination SPP results as well as the pseudorange residual comparison for METG between the general method and cIFB self-calibration method using broadcast ephemeris data for Aug 1, 2017, respectively. From Fig. 5, it can be seen that the GLONASS SPP time series with cIFB self-calibration are more stable than the results that do not utilize cIFB self-calibration. There is an obvious systematic bias in the pseudorange residual with no cIFB self-calibration, as seen in Fig. 6, and the periodic terms for the pseudorange residuals with no cIFB self-calibration can be eliminated by pseudorange cIFB self-calibration. The RMS accuracy of METG SPP, based on GLONASS broadcast ephemeris data, is found to improve from 3.42, 1.67, and 5.57 to 1.12 m, 1.06, and 3.05 m in the north, east, and up directions, respectively.

To best evaluate the effects and performance improvements from GLONASS cIFB self-calibration on GNSS SPP, the stations of Table 1 are re-analyzed using a different model, as follows:

- GLONASS SPP (GLS)
- GLONASS SPP with GFZ IFB calibration (GLS + GFZ)
- GLONASS SPP with cIFB self-calibration (GLS + cIFB)
- GPS + GLONASS (GPS + GLS)
- GPS + GLONASS with GFZ IFB calibration (GPS + GLS + GFZ)
- GPS + GLONASS with cIFB self-calibration (GPS + GLS + cIFB).

The GPS SPP is also presented for comparative analysis.

The bar chart in Fig. 7 presents the SPP RMS comparisons for GLS, GLS + GFZ, and GLS + cIFB. The lines present the improvement percentage for GLS + GFZ and GLS + cIFB, relative to a single GLONASS SPP. Taken from the results, it can be seen that there are indeed some contributions that the GLONASS IFB products provided by GFZ offer for several stations, with an average improvement percentage of 7.70 and 11.12% for horizontal and vertical directionality, respectively. Due to the accuracy of the IFB products from GFZ, some of the measures for station performance are found to still degrade to a significant extent.

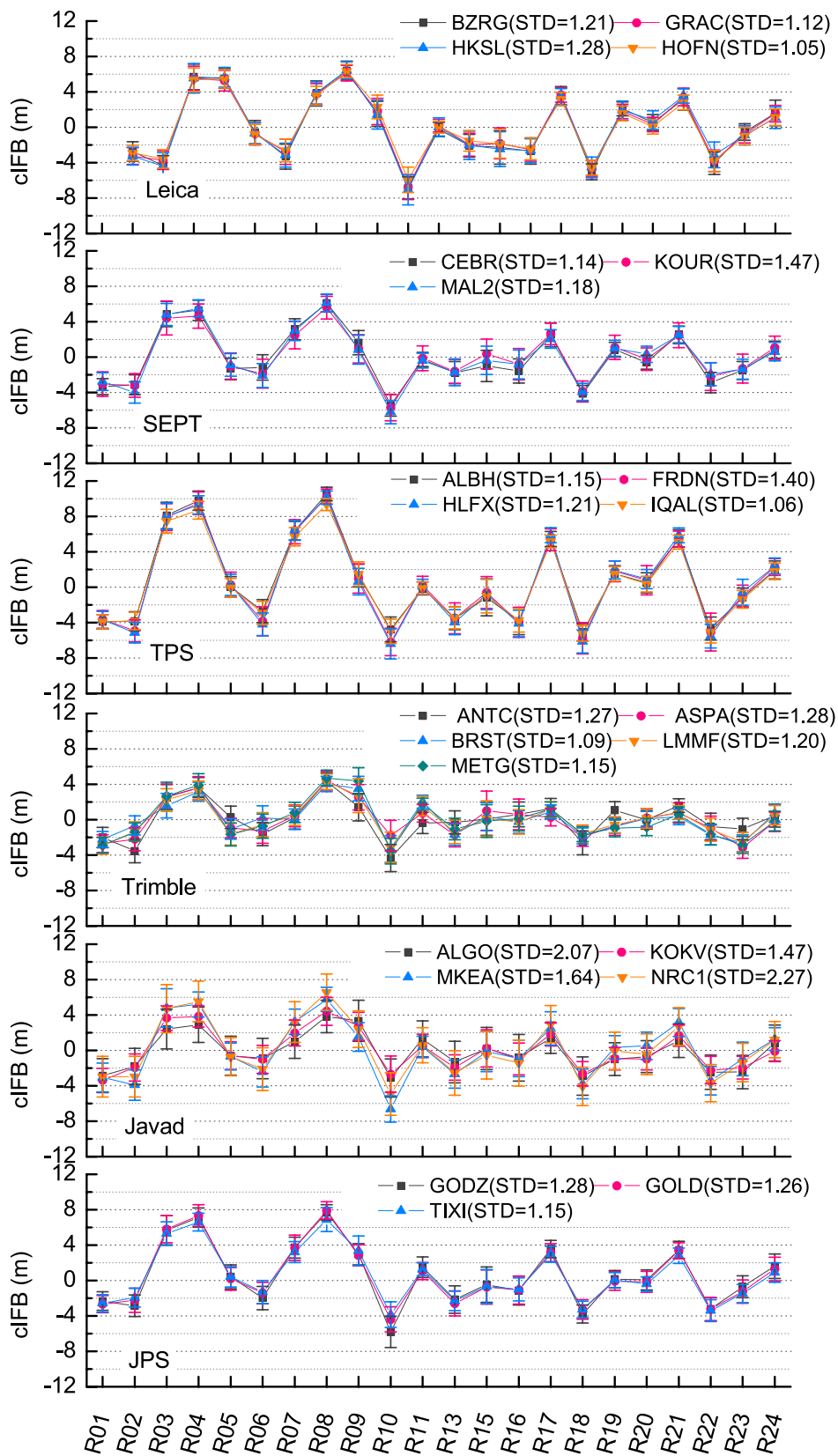


Fig. 3 Variation and standard deviation for cIFB as estimated by broadcast ephemeris data from DOY 200–300, 2017, for the 23 stations equipped with various manufacturer parts. Most of STDs are

less than 1.30 m, except for the stations equipped with Javad. According to the statistics, the average STD of all 23 stations is 1.32 m, which is limited by the broadcast ephemeris accuracy for GLONASS

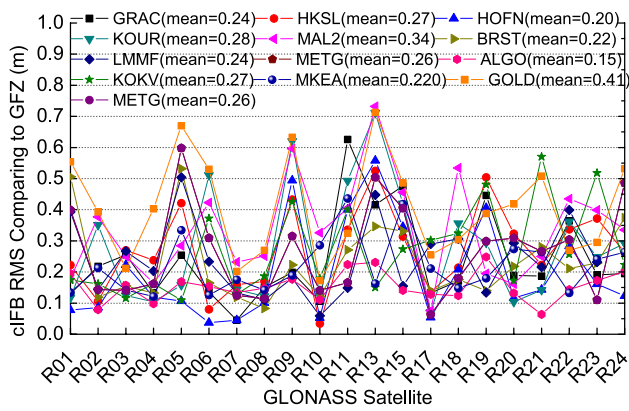


Fig. 4 GLONASS estimated cIFB RMS as compared with MGEX BIAS products provided by GFZ. Most RMS values are less than 0.6 m and the mean of the RMS for all stations and GLONASS satellites is 0.26 m

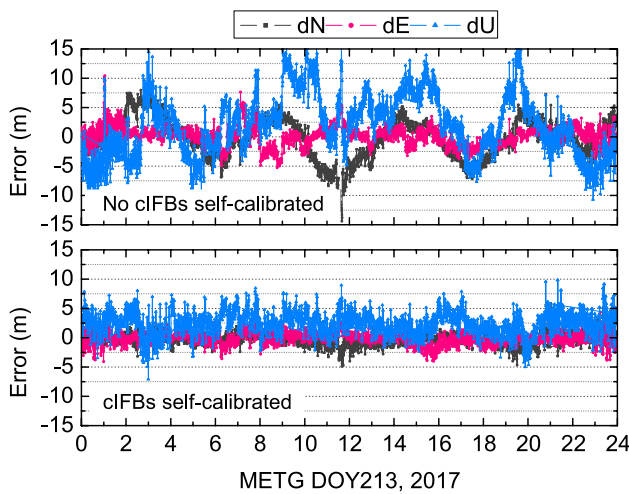


Fig. 5 GLONASS SPP results comparison between the standard method (top) and cIFB self-calibrated method using broadcast ephemeris data (bottom) for Aug 1, 2017

However, GLONASS positioning accuracy can be improved significantly using a cIFB self-calibration algorithm. As compared to a single GLONASS SPP, the average RMS of the GLONASS SPP retrieved from cIFB self-calibration is reduced from 4.63 and 7.61 m to 2.01 and 3.40 m in the horizontal and vertical direction, seeing an improvement of 54.18% and 53.80%, respectively.

The bar chart in Fig. 8 presents the SPP RMS comparison for GPS + GLS, GPS + GLS + GFZ, GPS + GLS + cIFB, and GPS. The lines presents the improvement percentage for GPS + GLS + GFZ and GPS + GLS + cIFB, relative to GPS + GLONASS SPP. From the results, it can be seen that the accuracy of GPS + GLONASS SPP can be additionally improved after GLONASS cIFB self-calibration to obtain 1.14 and 2.13 m in the horizontal and vertical direction with

an improvement percentage of 42.79% and 37.80%, respectively. For most stations, the accuracy of GPS + GLONASS SPP with GLONASS cIFB self-calibration is found to be better than with a single GPS SPP.

In addition, Fig. 7 and Fig. 8 also present the difference that GLONASS cIFB products provided by GFZ make to GLONASS point positioning. It is found that GLONASS positioning with GFZ IFB calibration can improve positioning accuracy for most stations from receiver-dependent GLONASS cIFB correction. However, satellite-dependent cIFB can still present itself in the residuals but can be eliminated by the cIFB self-calibration algorithm. Thus, integrating cIFB self-calibration can further improve GLONASS positioning accuracy via calibration in GFZ IFB products.

cIFB Self-calibration on PPP

The convergence rate of PPP at the initial period will depend on the accuracy of the pseudorange. This is because carrier phase ambiguities will not have yet been determined accurately (Geng et al. 2010b). Multi-GNSS fusion PPP can effectively accelerate convergence and improve stability significantly when compared to single GNSS PPP utilization (Chen et al. 2018). In order to analyze the effect of GLONASS cIFB on PPP, PPP with estimating cIFB parameters is carried out in this section.

The use of GFZ precision products for PPP leads only to receiver-dependent cIFB in observations. The GLONASS IFB products provided by GFZ are very suitable for cIFB calibration in PPP. Figure 9 shows the convergence period comparison for single GPS PPP, GPS + GLONASS fusion PPP, GPS + GLONASS fusion PPP with estimating cIFB, and GPS + GLONASS fusion PPP with GFZ IFB calibration for the station ALGO. Figure 10 shows that the convergence time statistics under the condition of the three-dimensional (3D) error less than 10 cm. From the figure, it can be seen that GPS + GLONASS fusion PPP can improve convergence time from about 40 min to about 20 min in the case of station BRST. From Fig. 10, it is found that the convergence time improvement percentage for GPS + GLONASS + cIFB and GPS + GLONASS + GFZ, relative to GPS, is 58.62 and 50.81%, respectively. The average improvement percentage for GFZ cIFB calibration, relative to GPS + GLONASS, is about 12.59% when neglecting the station ALGO. The accuracy of ALGO with GFZ cIFB calibration decline significantly, which may be caused by the poor accuracy of GLONASS cIFB.

As analyzed above, GLONASS cIFB significantly changes with the receiver hardware used. GLONASS cIFB self-estimation can achieve good self-consistency between cIFB and station, which can further promote convergence efficiency for most stations relative to GPS + GLONASS PPP, by average improvement percentage of 19.03%.

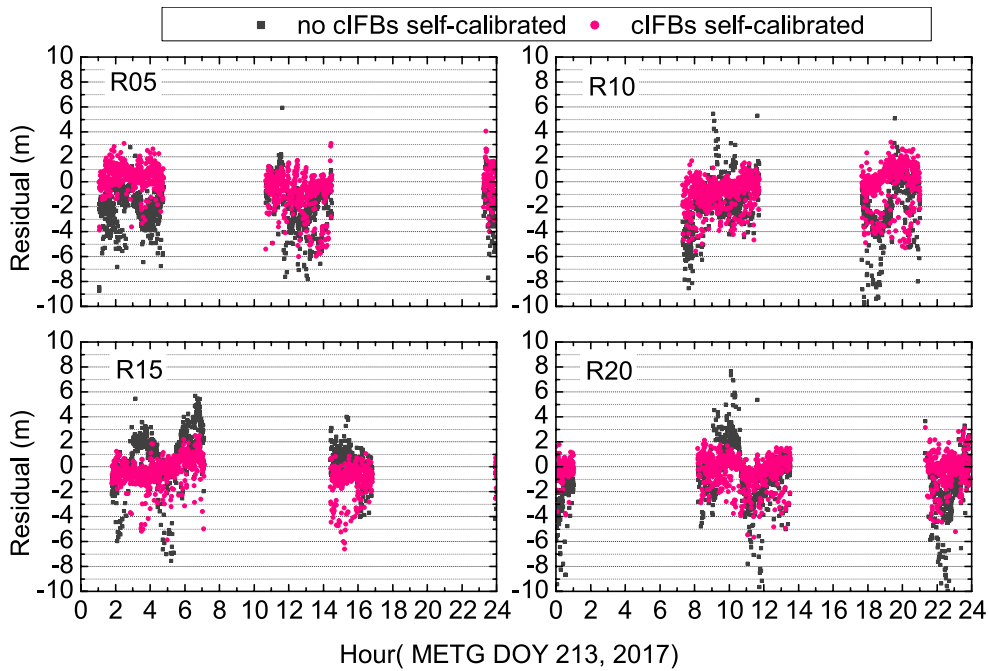


Fig. 6 METG pseudorange residual time series for GLONASS R05, R10, R15, and R20 for Aug 1 (DOY 213), 2017 (UTC)

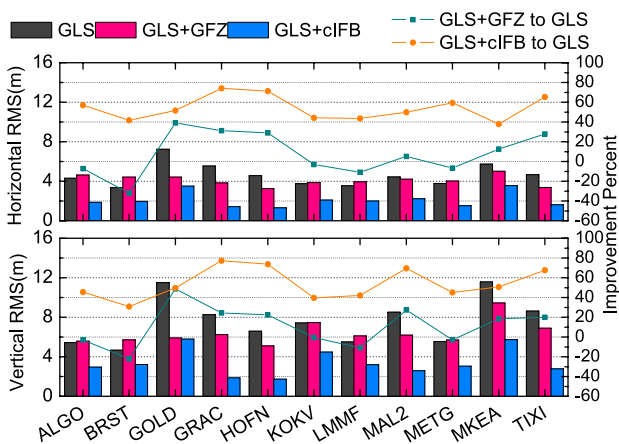


Fig. 7 Bar chart presenting the SPP RMS comparison between GLONASS, GLONASS with GFZ IFB calibration, and GLONASS with cIFB self-calibration. The line represents the improvement percentage for GLONASS + GFZ and GLONASS + cIFB relative to a single GLONASS SPP. In the percentage A relative to B, the numerator is B minus A, and the denominator is B

The positioning accuracy after convergence in the four solution modes is also analyzed, and the results are presented in Fig. 11. Here it can be seen that the GPS + GLONASS fusion

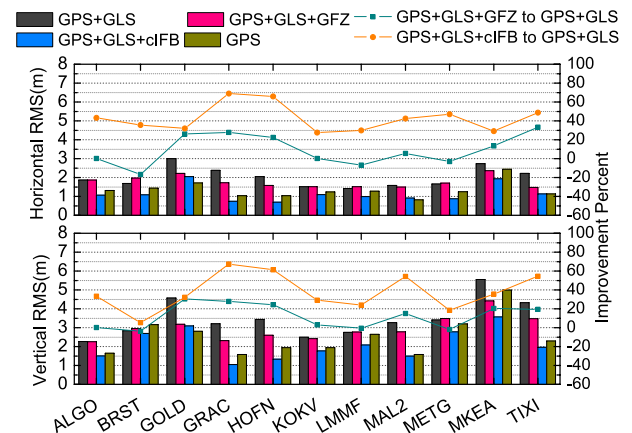


Fig. 8 Bar chart presenting the SPP RMS comparisons for GPS + GLONASS, GPS + GLONASS with GFZ IFB calibration, and GPS + GLONASS with cIFB self-calibration. The lines represent improvement percentage, relative to GPS + GLONASS SPP

PPP can improve positioning accuracy when compared to single GPS PPP. In addition, GPS + GLONASS PPP with cIFB self-calibration can achieve the same accuracy with GPS + GLONASS PPP. This is a result of the ability of the carrier phase to determine positioning accuracy after ambiguity convergence. However, it must be noted that the accuracy of GPS + GLONASS PPP with GFZ cIFB calibration is found to be slightly worse when compared with GPS + GLONASS fusion PPP. This may be attributable to the poor accuracy of GLONASS cIFB.

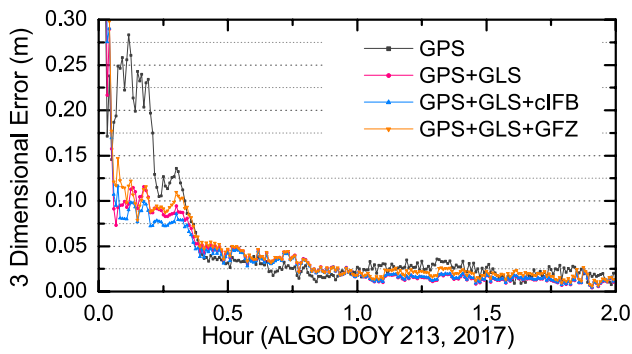


Fig. 9 3D Convergence comparison for GPS PPP, GPS+GLONASS PPP, GPS+GLONASS+cIFB PPP, and GPS+GLONASS+GFZ PPP of ALGO station

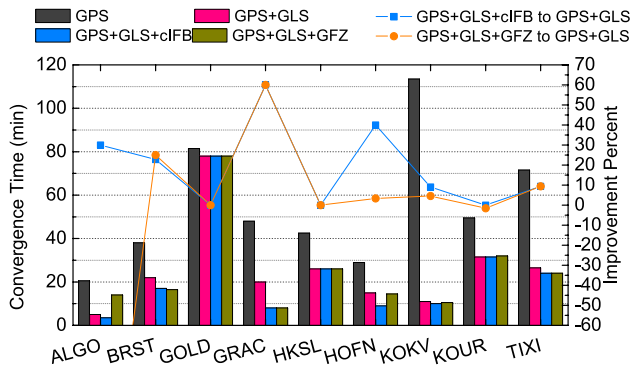


Fig. 10 Comparison for GPS, GPS + GLONASS fusion, GPS + GLONASS+cIFB and GPS + GLONASS+GFZ PPP convergence time under condition of 3D error less than 10 cm

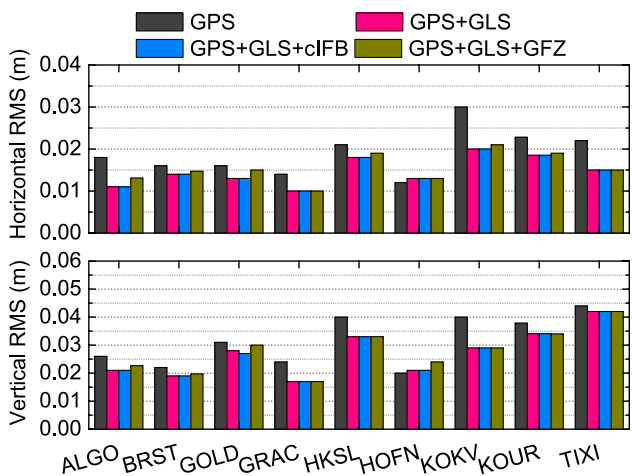


Fig. 11 RMS statistics after converging GPS PPP, GPS+GLONASS fusion PPP, GPS+GLONASS+cIFB PPP, and GPS+GLONASS+GFZ IFB PPP

Conclusion

To analyze the characteristic of GLONASS code inter-frequency bias and its effects on positioning, an estimation model and data process strategy for GLONASS cIFB in multi-GNSS fusion positioning and single GLONASS positioning was presented to realize GLONASS cIFB real-time self-calibration using a single station. A total of 23 stations equipped with various manufacturer hardware were used to analyze the characteristics of GLONASS cIFB and its relationship with the different receiver hardware. The results can be summarized as follows:

1. There is an obvious common trend in the cIFB estimated by broadcast ephemeris data for all the different sample manufacturers, and the unequal GLONASS inter-satellites cIFB of the same brand manufacturer were found to change significantly.
2. A good consistency was found between self-calibrated receiver-dependent GLONASS cIFB and GFZ IFB products.
3. The algorithm for cIFB real-time self-calibration not only corrects receiver-dependent cIFB, but also further eliminates satellite-dependent cIFB, which provides more stable results, further improving the accuracy of GNSS point positioning significantly when including GLONASS satellites, as compared to SPP with GFZ IFB calibration. It was found that the RMS of single GLONASS SPP can be improved from 4.63 and 7.61 m in the horizontal and vertical direction, representing 54.18 and 53.80% improvement, respectively. For GPS + GLONASS SPP, the RMS with cIFB self-calibration was found to be capable of improving to 1.14 and 2.13 m in the horizontal and vertical direction implying an improvement percentage of 42.79 and 37.80%, respectively.
4. GLONASS cIFB self-estimation was found to be able to achieve good self-consistency between cIFB and station, which further promotes convergence efficiency, relative to GPS + GLONASS PPP, achieving on average an improvement percentage of 19.03%. This accuracy is nearly consistent with that of GPS + GLONASS fusion PPP.
5. The algorithm for GLONASS cIFB self-calibration is recommended for real-time navigation and for improving the availability and stability of GNSS positioning.

Acknowledgements We thank Dr. Ge Maorong of the German Research Centre for Geosciences (GFZ) for his many suggestions and guidance. This research is sponsored by National Natural Science Foundation (Grant No. 41574027, 41574030, 41604029, 41774035 and 61501430), National Key Research and Development Plan (Grant No.

2016YFB0501802), and Wuhan Morning Light Plan of Youth Science and Technology (Grant No.2017050304010301).

References

- BeiDou SISICD (2017) BeiDou navigation satellite system signal in space interface control document open service signal (Version 2.1)
- Bierman GJ (1977) Factorization methods for discrete sequential estimation. Academic Press Inc., New York, 1977
- Chen L, Zhao Q, Hu Z, Jiang X, Geng C, Ge M, Shi C (2018) GNSS global real-time augmentation positioning: Real-time precise satellite clock estimation, prototype system construction and performance analysis. *Adv Space Res* 61(1):367–384
- Dach R, Schaer S, Hugentobler U (2006) Combined multi-system GNSS analysis for time and frequency transfer. In: Proceedings of the 20th European Frequency and Time Forum EFTF06, 2006, Braunschweig, Germany, pp 530–537
- Deng Z, Nischan T, Bradke M (2017) Multi-GNSS rapid orbit-, clock- & EOP-product series. GFZ Data Services
- Galileo OS SIS ICD (2016) European GNSS (Galileo) Open service signal-in-space interface control document, 2016
- Ge M, Gendt G, Rothacher M, Shi C, Liu J (2008) Resolution of GPS carrier phase ambiguities in precise point positioning (PPP) with daily observations. *J Geod* 82(7):389–399
- Ge Y, Zhou F, Sun B, Wang S, Shi B (2017) The impact of satellite time group delay and inter-frequency differential code bias corrections on multi-GNSS combined positioning. *Sensors* 17(3):602–721
- Geng J, Meng X, Dodson AH, Teferle FN (2010a) Integer ambiguity resolution in precise point positioning: method comparison. *J Geod* 84(9):569–581
- Geng J, Meng X, Dodson AH, Ge M, Teferle FN (2010b) Rapid reconvergences to ambiguity-fixed solutions in precise point positioning. *J Geod* 84(12):705–714
- GLONASS ICD (2008) GLONASS interface control document in bands L1, L2 (Edit 5.1), 2008
- Hatch R (1982) The synergism of GPS code and carrier measurements. Proceedings of the Third International Symposium on Satellite Doppler Positioning at Physical Sciences Laboratory of New Mexico State University, Feb. 8–12, Vol. 2, pp 1213–1231
- IS-GPS-200G (2013) Global positioning system directorate systems engineering & integration interface specification
- Li X, Ge M, Zhang H, Wickert J (2013) A method for improving uncalibrated phase delay estimation and ambiguity-fixing in real-time precise point positioning. *J Geod* 87(5):405–416
- Li X, Ge M, Dai X, Ren X, Fritsche M, Wickert J, Schuh H (2015) Accuracy and reliability of multi-GNSS real-time precise positioning: GPS, GLONASS, BeiDou, and Galileo. *J Geod* 89(6):607–635
- Montenbruck O, Steigenberger P, Prange L, Deng Z, Zhao Q, Perosanz F, Romero I, Noll C, Stürze A, Weber G, Schmid R, MacLeod K, Schaer S (2017) The multi-GNSS experiment (MGEX) of the international GNSS service (IGS) - achievements, prospects and challenges. *Adv Space Res* 59(7):1671–1697
- Shi C, Yi W, Song W, Lou Y, Yao Y, Zhang R (2013) GLONASS pseudorange inter-channel biases and their effects on combined GPS/GLONASS precise point positioning. *GPS Solut* 17(4):439–451
- Wanninger L (2012) Carrier-phase inter-frequency biases of GLONASS receivers. *J Geod* 86(2):139–148
- Wanninger L, Wallstab-Freitag S (2007) Combined processing of GPS, GLONASS, and SBAS code phase and carrier phase measurements. In: Proceedings ION GNSS-2007. Institute of Navigation, Fort Worth, Texas, pp 866–875
- Zumberge J, Heflin M, Jefferson D, Watkins M, Webb F (1997) Precise point positioning for the efficient and robust analysis of GPS data from large networks. *J Geophys Res* 102(B3):5005–5017

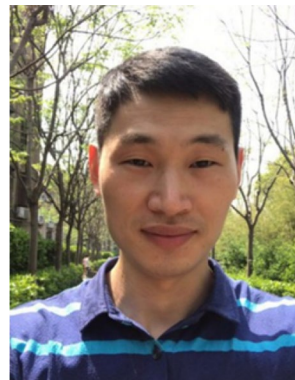


(POD), and GNSS wide-area augmentation.

Liang Chen is currently a Ph.D. student at the GNSS Research Center at Wuhan University in China. In addition, he is also an associate researcher at the China Academy of Aerospace Electronics Technology. He received his master degree at Wuhan University in 2012 and visited the GFZ German Research Centre for Geosciences as an academic scholar in 2016. Chen Liang's current research focuses primarily on multi-GNSS PPP, real-time precise clock estimation, precise orbit determination



Min Li is a professor at the GNSS Research Center at Wuhan University in China. He received his master's degree and doctorate from Wuhan University in 2007 and 2011, respectively. The focus of Dr. Li's current research lies in precise orbit determination for GNSS.



Zhigang Hu is an associate professor at the GNSS Research Center at Wuhan University in China. He received his master's degree and doctorate from Wuhan University in 2008 and 2013, respectively. The focus of Dr. Hu's current research lies in precise orbit determination for GNSS as well as performance evaluation for the BeiDou satellite navigation system.



Chenghe Fang is currently an engineer at the China Academy of Aerospace Electronics Technology in China. He received his master's degree from Hohai University in 2017. His current research focuses primarily on positioning, monitoring, and assessment for satellite navigation.



Qile Zhao is a professor at the GNSS Research Center at Wuhan University in China. He received his Ph.D. degree from Wuhan University in 2004. In 2006-2007, Dr. Zhao completed his postdoctoral program at the Delft University of Technology in the Netherlands. His current research interests are precise orbit determination for GNSS and low earth orbit satellites, as well as high-precision positioning using GPS, Galileo, and the BeiDou satellite navigation system.



Changjiang Geng is currently an associate researcher at the China Academy of Aerospace Electronics Technology in China. He obtained his Ph.D. from Wuhan University in 2011. His current research focuses primarily on ionosphere models and methods for evaluating the performance of GNSS service.



Chuang Shi is a professor at Beihang University in China. He graduated from Wuhan University and obtained his Ph.D. degree in 1998. Dr. Shi's research interests include network adjustment, precise orbit determination for GNSS satellites and LEOs, as well as real-time PPP.